COMPARING THE MY25 AND MY34 GLOBAL DUST STORMS USING THE ENSEMBLE MARS ATMOSPHERE REANALYSIS SYSTEM (EMARS)

N. Polek-Davis, *Department of Meteorology and Atmospheric Science, The Pennsylvania State University, University Park, PA, USA (ntp5125@psu.edu)*, **S. J. Greybush**, *Department of Meteorology and Atmospheric Science, The Pennsylvania State University, University Park, PA, USA*, **R. J. Wilson**, *Space Science and Astrobiology Division, NASA Ames Research Center, Moffett Field, CA, USA*, **R. P. McMichael**, *Department of Meteorology and Atmospheric Science, The Pennsylvania State University, University Park, PA, USA*, **H. E. Gillespie**, *Lunar and Planetary Institute, Universities Space Research Association, Houston, TX, USA.*

Introduction: The analysis of dust storms is crucial towards understanding Martian weather and climate. Using the Ensemble Mars Atmosphere Reanalysis System (EMARS; Greybush et al., 2019), this study builds upon that understanding by conducting a comparative analysis between two global dust storms.

While regional dust storms occur on Mars every year, every ~3-5 years one of these storms evolves into a global dust storm (GDS). The MY 25 GDS began around Ls 177˚ as local dust storms along the northwestern rim of Hellas Basin, expanded to the east and north, and encircled the planet by Ls 193˚ (Strausberg et al., 2005; Wolkenberg et al., 2020; Wang et al., 2015). The MY 34 GDS began around Ls 185˚ in Acidalia around 10˚E, 60˚N, expanded westward and equatorward, and covered Mars by Ls 193˚ (Gillespie et al., 2020). In both MY25 and MY34, common features include the eastward expansion of the two storms from local lifting of the tropics, and the initiation of multiple dust-lifting centers that were dynamically active throughout the onset and progression of the storm (Bertrand et al., 2020). Despite similar explosive growth and season of occurrence, the origin locations of these storms differ significantly, with the MY 25 GDS beginning in the southern hemisphere and the MY 34 GDS in the north. In addition, the exact circumstances that dictate whether a storm remains regional or expands globally are not yet understood. To connect dust in the atmosphere to the winds that lift it, we examine surface wind stress and dust opacity. Several comparisons of these factors have been made between MY 25 and years without global dust storms (e.g. Montabone et al., 2005; Kass et al., 2016; Wolkenburg et al., 2020), but no comparisons have yet been made between the MY 25 and MY 34 storms using EMARS.

EMARS assimilates retrievals from the IR Thermal Emission Spectrometer (TES) and Mars Climate Sounder (MCS) to form a temporal gridded dataset representing a variety of atmospheric variables. EMARS dust field and wind stress fields are compared with visible satellite imagery from the Mars Orbital Camera (MOC). Then the dust opacity and wind stress values are extracted and compared at three different time periods, as well as analyzed relative to non-global dust storm years in order to identify global dust storm characteristics and behavior.

Data and Methods: EMARS directly assimilates temperature retrievals from the Thermal Emission Spectrometer (TES; Christensen et al., 2001) and Mars Climate Sounder (MCS; McCleese et al., 2007) instruments using the Local Ensemble Transform Kalman Filter (LETKF) method (Hunt et al., 2007) within the GFDL/NASA Mars Global Climate Model
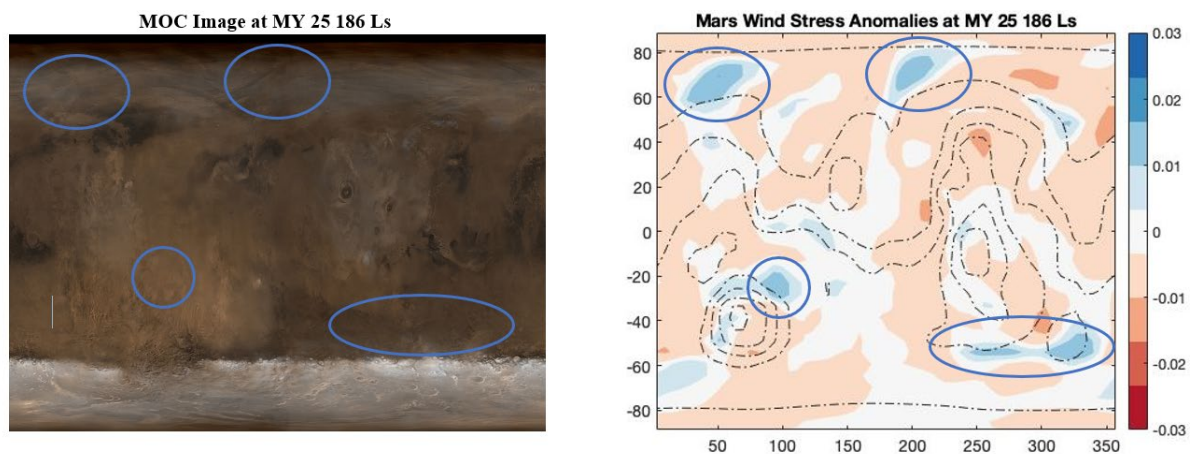
Figure 1. MOC (left) and EMARS wind stress anomaly (right; N/m^2) comparison at MY 25 Ls 186º. Blue circles highlight areas where EMARS predicts substantial positive wind stress anomalies, and black dotted lines indicate Martian topography. MOC imagery courtesy of NASA/MSSS.
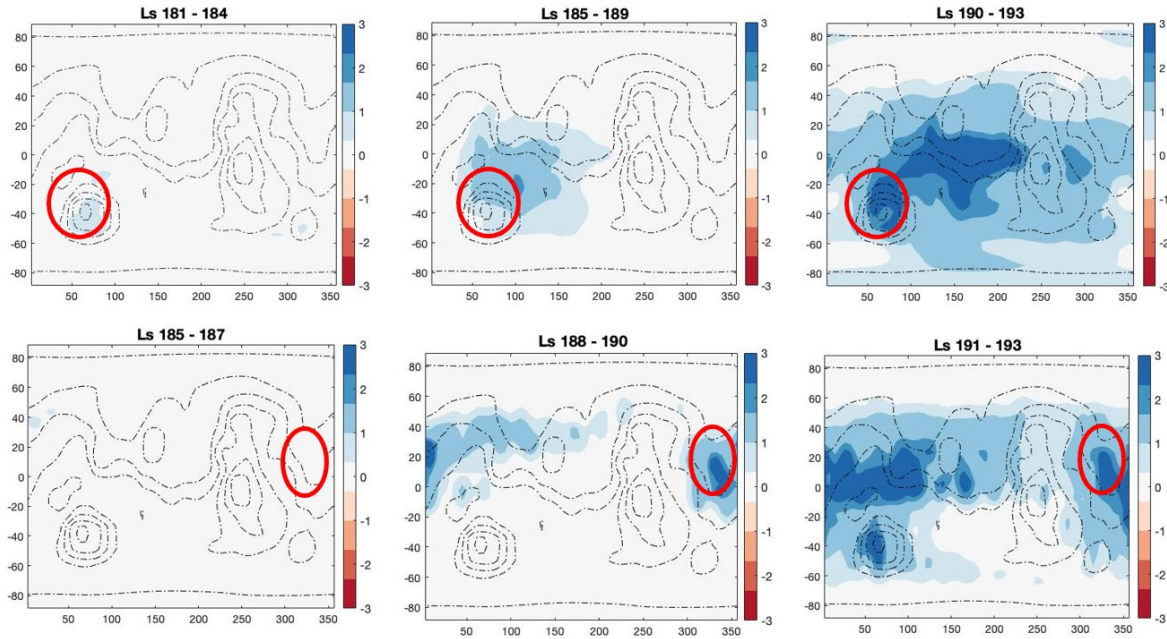
Figure 2. Latitude-longitude maps of dust opacity differences measured in units of number density and averaged over three different periods (columns). Dotted overlay represents Martian topography. Observed origin locations of each storm are circled in red. Top row: MY 25 subtracted by MY 24 values. Blue/positive value areas indicate higher dust opacity in MY 25. Bottom row: MY 34 subtracted by MY 30 values. Blue/positive value areas indicate higher dust opacity in MY 34.

(MGCM) to provide a best estimate of the Martian atmospheric state at any hour from the middle of MY 24 to the beginning of MY 34 (with a gap in MY27/28 between the TES and MCS eras). For the purposes of this project, the variables extracted from EMARS are dust opacity and wind stress. The horizontal dust column opacity fields are strongly driven by the Montabone et al. (2015) dust products, which are originally derived from TES and MCS observations. For MY 34, the dust maps are derived from the updated methodology in Montabone et al. (2020), which uses the 2-D v5.3.2 MCS dust retrievals. MOC imagery (Malin et al., 1992; Cantor et al., 2007) is then used to provide an independent view of the dust storm through visible imagery.

On Mars, dust and wind stress are codependent; wind stress and convection impact dust lifting, and dust's impact on temperature affects convection, wind patterns, and wind stress (Haberle et al., 2006). There have been a variety of methods proposed to attempt to address this relationship in a model (Kahre et al., 2006; Basu et al., 2004; Newman et al., 2015); however, further development of this relationship in the context of Mars would be a valuable improvement. While the MGCM has the functionality to apply a wind stress lifting scheme, EMARS does not currently employ this option as the wind stress values must first be validated before such a relationship can be confidently employed. One of the aims of this research is to validate the wind stress values of EMARS

such that the dust-wind relationship can be utilized within EMARS for future work.

For this study we are most interested in the anomalous meteorological factors contributing to global dust storm formation, rather than repeatable patterns of dust lifting and dust opacity. We can therefore define the non-GDS data for TES and MCS as an average of their respective data during the periods within which these observations are available: MY 24 and MY 26 for TES, and MY 30 and MY 31 for MCS. We then subtract the non-GDS data from the GDS years for each respective instrument in order to highlight the anomalous data and remove any biases from differences in instrument characteristics and assimilation of these datasets. Finally, EMARS anomaly fields can be compared between the two storms.

MOC Imagery and EMARS Comparison: We compared MOC imagery to EMARS dust (not shown) and wind stress anomalies (Figure 1) at a variety of times (only one time depicted in Figure 1). EMARS dust compares favorably to MOC imagery in most locations during the growth phase of the MY25 GDS. In Figure 1, we can also see a generally favorable comparison of positive wind stress anomalies with areas of potentially active dust lifting: near Hellas, Argyre, and in the Northern high latitudes. The wind stress anomalies at these high latitudes are likely associated with baroclinic wave activity. Many, but not
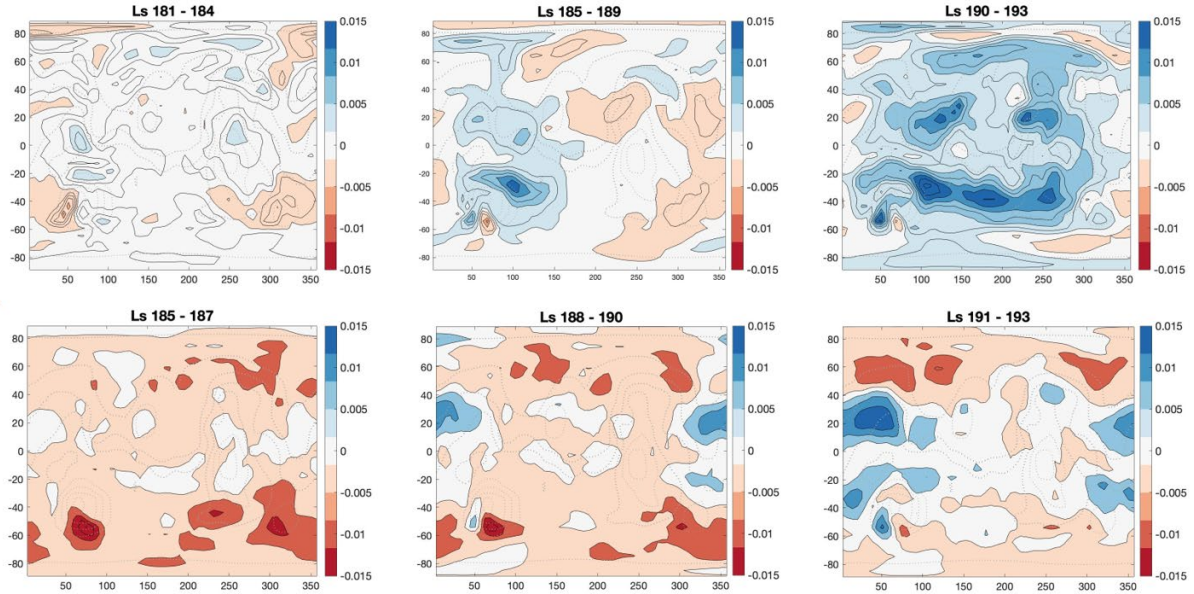
Figure 3. Latitude-longitude maps of wind stress differences measured in N/m^2 and averaged over three different periods (columns). Dotted overlay represents Martian topography. Top row: MY 25 subtracted by MY 24 values. Blue/positive value areas indicate higher wind stress in MY 25. Bottom row: MY 34 subtracted by MY 30 values. Blue/positive value areas indicate higher wind stress in MY 34.

all, areas of likely dust lifting are captured by positive wind stress anomalies.

Dust Storm Comparison: Both the dust opacity (Figure 2) and the wind stress (Figure 3) display major differences between non-GDS and GDS years. Figure 2 shows the total dust opacity difference between MY 24 and 25, both in the TES era; as well as MY 30 and 34, both in the MCS era. Within EMARS, the dust disparity is most clearly seen at 50° E, 60° S for MY 25, and 10° E, 40° N for MY 34. This matches up with observations of the storms' original lifting centers (Montabone et al., 2005; Gillespie et al., 2020). The dust opacity then increases in both intensity and spread for both cases, with the MY 25 GDS expanding northeast, and the MY 34 GDS progressing southwest. The latitudinal movement is likely due to the Hadley circulation of the Martian atmosphere, expanding in different directions depending on the initial location of the dust. Once the dust has been transported sufficiently northwards, the jet stream carries it eastward to allow it to encircle the planet (Gillespie et al., 2020). Figure 3 shows that both storms show positive wind stress anomalies in the region of initial lifting, but that the MY25 storm has more significant wind stress anomalies that extend across a larger portion of the planet. This encourages exploration of the triggering of dust lifting centers at additional locations.

Conclusions: This work compares EMARS dust opacity and wind stress anomalies for MY25 with MOC visible imagery and notes a reasonable correspondence to areas of likely active dust lifting. Dust opacity anomalies for MY25 and MY34 show the differences in progression for the two storms, despite beginning at a very similar time of year. While both storms feature wind stress anomalies near the origin points for the storms, differences between the two storms indicate stronger anomalies in MY25, with a greater connection to multiple lifting centers across the planet. Instrumentation-related differences in EMARS between the TES and MCS eras, particularly how the instruments view the atmosphere (and penetrate the veil of dust to view the lower atmosphere) and how this information is assimilated, should also be considered in comparative analyses of these storms.

References:
Basu, S., et al., Simulation of the Martian Dust Cycle with the GFDL Mars GCM, *J. Geophys. Res. Planets*, *109*(E11), 2004.
Bertrand, T. et al., Simulation of the 2018 Global Dust Storm on Mars Using the NASA Ames Mars GCM: A Multitracer Approach, *J. Geophys. Res. Planets*, 125, 7, 2020.

Cantor, B. A., MOC observations of the 2001 Mars Planet-encircling dust storm, *Icarus*, *186*(1), 60-96, 2007.

Christensen, P. R., et al., Mars Global Surveyor Thermal Emission Spectrometer experiment: Investigation description and surface science results, *J. Geophys. Res.*, *106*(E10), 23823, 2001.

Gillespie, H. E., et al., An investigation of the encirclement of Mars by dust in the 2018 global dust storm using EMARS, *J. Geophys. Res Planets, 125*(7), 2020.

Greybush, S. J., et al., The Ensemble Mars Atmosphere Reanalysis System (EMARS) Version 1.0, *Geosci. Data J.*, *6*(2), 137–150, 2019.

Haberle, R. M., et al., Role of Dust Devils and Orbital Precession in Closing the Martian Dust Cycle, *Geophys. Res. Lett.*, *33*(19), 2006.

Hunt, B. R., et al., Efficient data assimilation for Spatiotemporal Chaos: A local ensemble transform Kalman filter, *Phys. D: Nonlinear Phenom.*, *230*(1-2), 112-126, 2007.

Kahre, M. A., et al., Modeling the Martian Dust Cycle and Surface Dust Reservoirs with the NASA Ames General Circulation Model, *J. Geophys. Res.*, *111*(E6), 2006.

Kass, D. M., et al., Interannual Similarity in the Martian Atmosphere during the Dust Storm Season, *Geophys. Res. Lett.*, *43*(12), 6111-6118, 2016.

Malin, M. C., et al., Mars observer camera, *J. Geophys. Res.*, *97*(E5), 7699, 1992.

McCleese, D. J., et al., Mars Climate Sounder: An investigation of thermal and water vapor structure, dust and condensate distributions in the atmosphere, and energy balance of the polar regions, *J. Geophys. Res., 112*(E5), 2007.

Montabone, L., et al., Interannual variability of Martian dust storms in assimilation of several years of mars global surveyorobservations, *Adv. Space Res.*, *36*(11), 2146-2155, 2005.

Montabone, L. et al. (2015), Eight-year climatology of dust optical depth on Mars, Icarus, 251, 65–95, doi:10.1016/j.icarus.2014.12.034.

Montabone, L., A. Spiga, D. M. Kass, A. Kleinböhl, F. Forget, and E. Millour (2020), Martian year 34 column Dust Climatology from Mars Climate Sounder Observations: Reconstructed maps and model simulations, Journal of Geophysical Research: Planets, 125(8), doi:10.1029/2019je006111.

Newman, C. E. and M. I. Richardson, The Impact of Surface Dust Source Exhaustion on the Martian Dust Cycle, Dust Storms and Interannual Variability, as Simulated by the MARSWRF General Circulation Model, *Icarus*, *257*, 47-87, 2015.

Strausberg, M. J., et al., Observations of the Initiation and Evolution of the 2001 Mars Global Dust Storm, *J. Geophys. Res.*, *110*(E2), 2005.

Wang, H., and M. I. Richardson, The origin, evolution, and trajectory of large dust storms on Mars during Mars years 24-30 (1999-2011), *Icarus*, *251*, 112-127, 2015.

Wolkenberg, P., et al., Similarities and differences of global dust storms in MY 25, 28, and 34, *J. Geophys. Res. Planets*, *125*(3), 2020.